US008446045B2

(12) **United States Patent**
Smith et al.

(10) **Patent No.: US 8,446,045 B2**
(45) **Date of Patent: May 21, 2013**

(54) **FLAT, ASYMMETRIC, AND E-FIELD CONFINED WIRELESS POWER TRANSFER APPARATUS AND METHOD THEREOF**

(75) Inventors: **Joshua R. Smith**, Seattle, WA (US); **Alanson P. Sample**, Seattle, WA (US); **Emily B. Cooper**, Seattle, WA (US)

(73) Assignee: **Intel Corporation**, Santa Clara, CA (US)

(*) Notice: Subject to any disclaimer, the term of this patent is extended or adjusted under 35 U.S.C. 154(b) by 776 days.

(21) Appl. No.: **12/544,956**

(22) Filed: **Aug. 20, 2009**

(65) **Prior Publication Data**

US 2010/0052811 A1 Mar. 4, 2010

Related U.S. Application Data

(60) Provisional application No. 61/189,502, filed on Aug. 20, 2008.

(51) **Int. Cl.**
H01F 27/42 (2006.01)
H01F 37/00 (2006.01)

(52) **U.S. Cl.**
USPC **307/104**

(58) **Field of Classification Search**
USPC 307/104
See application file for complete search history.

(56) **References Cited**

U.S. PATENT DOCUMENTS

6,498,557	B2 *	12/2002	Johnson	336/200
7,262,700	B2 *	8/2007	Hsu	340/572.1
7,649,283	B2 *	1/2010	Tonn et al.	307/104
7,709,732	B2 *	5/2010	Phillips	174/36
2007/0032274	A1	2/2007	Lee et al.	
2008/0278264	A1	11/2008	Karalis et al.	
2009/0051224	A1 *	2/2009	Cook et al.	307/104
2009/0152954	A1	6/2009	Le et al.	
2012/0001492	A9	1/2012	Cook et al.	

FOREIGN PATENT DOCUMENTS

KR 2002-0007117 A 1/2002

OTHER PUBLICATIONS

International Search Report with Written Opinion corresponding to international application No. PCT/US2010/048628, dated May 20, 2011, 7 pages.

* cited by examiner

Primary Examiner — Hal Kaplan
(74) *Attorney, Agent, or Firm* — Pillsbury Winthrop Shaw Pittman LLP

(57) **ABSTRACT**

In accordance with various aspects of the disclosure, a method and apparatus is disclosed that includes feature of a transmitter and receiver having a substantially two-dimensional resonator structure including a flat coil; and an impedance-matching structure operably connected to the resonator structure, the transmitter configured to transmit power wirelessly.

23 Claims, 9 Drawing Sheets

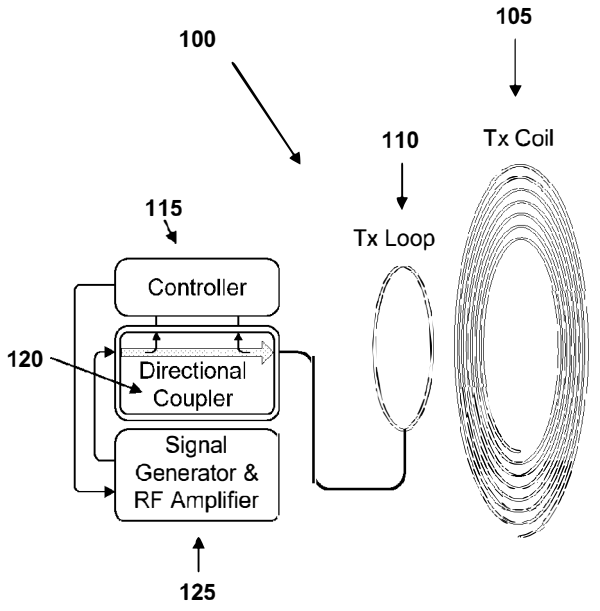

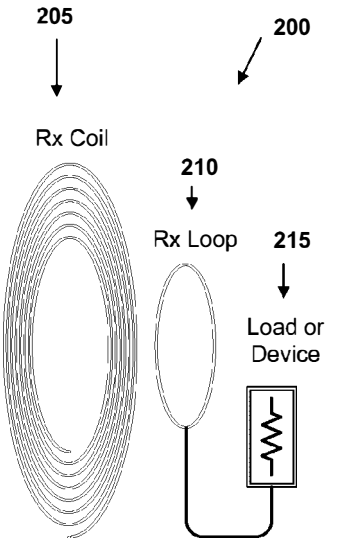

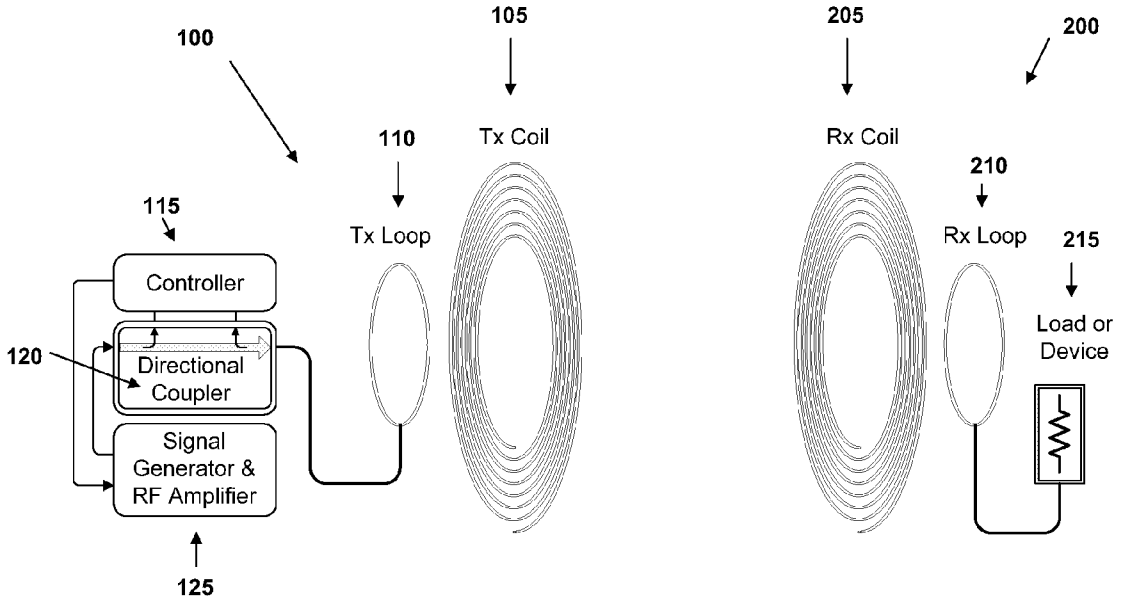
100
105
205
200
110
Tx Coil
Rx Coil
210
115
Tx Loop
Rx Loop
215
Controller
Load or
Device
120
Directional
Coupler
Signal
Generator &
RF Amplifier
125

Figure 1a

FIGURE 1b

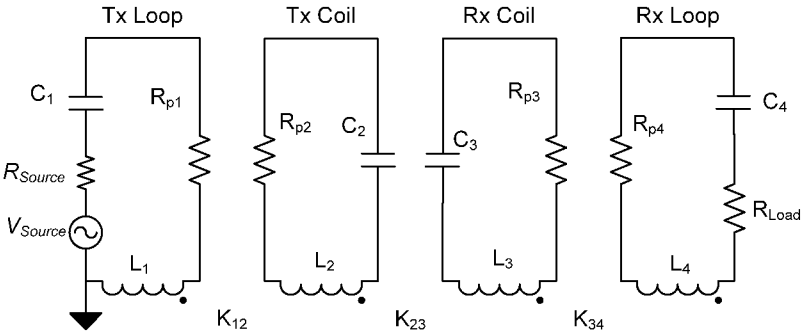

FIGURE 1c

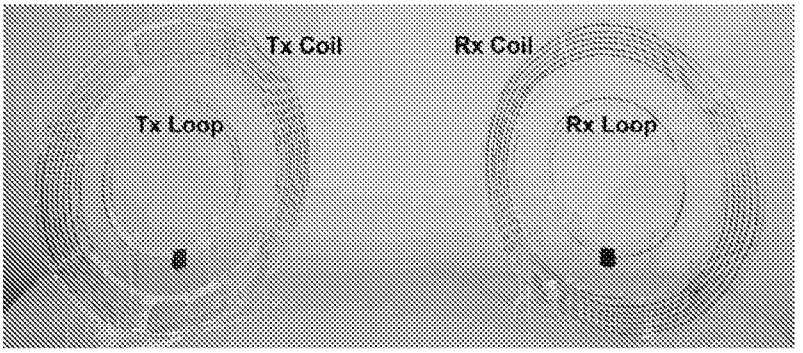

FIGURE 2a

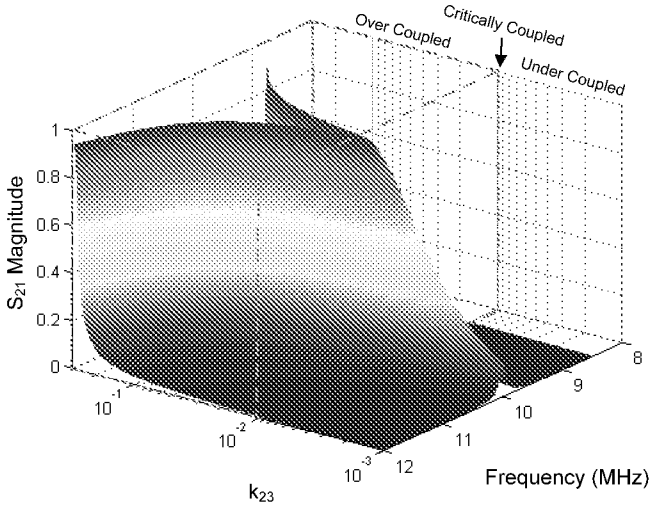

FIGURE 2b

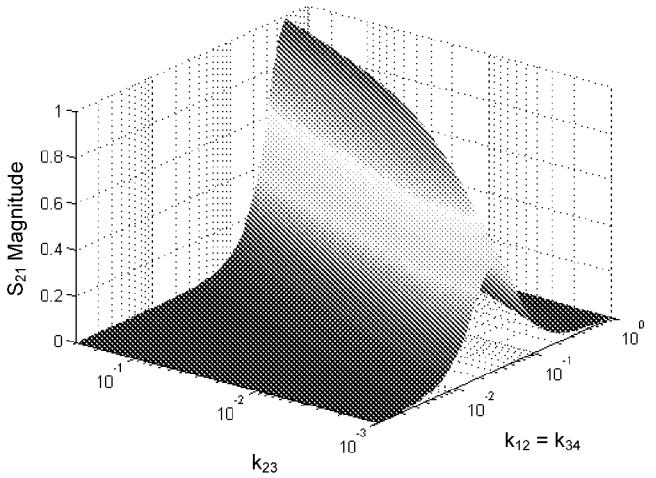

FIGURE 3a

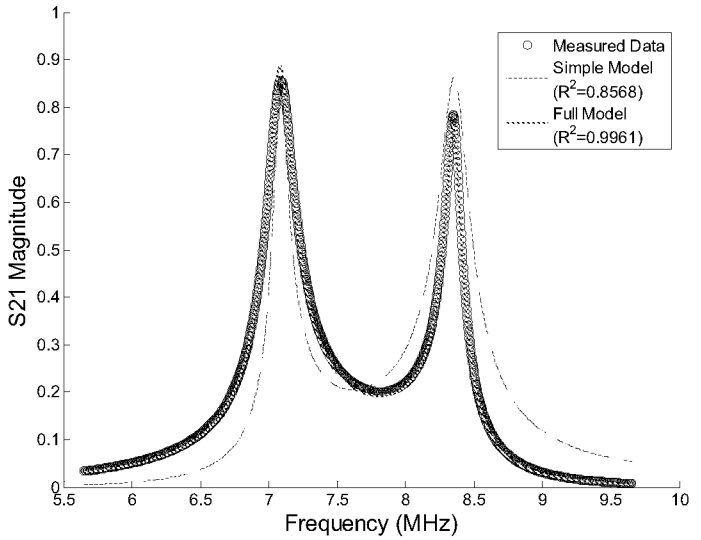

FIGURE 3b

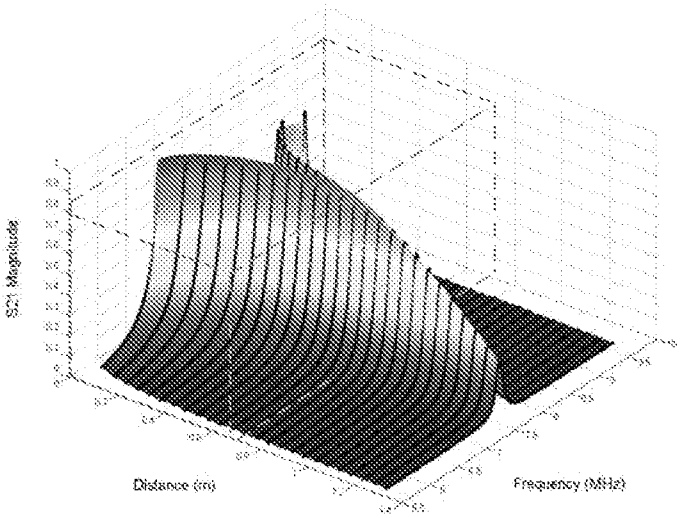

FIGURE 4a

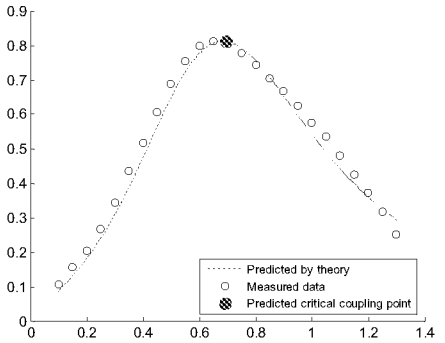

FIGURE 4b

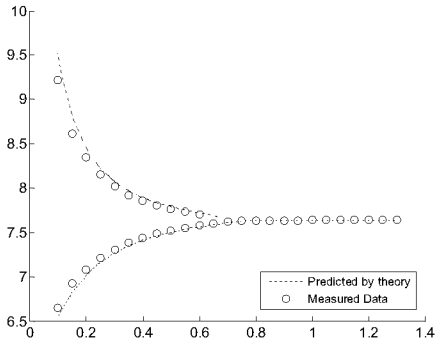

FIGURE 4c

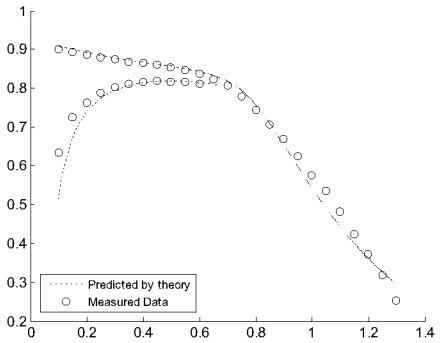

FIGURE 5

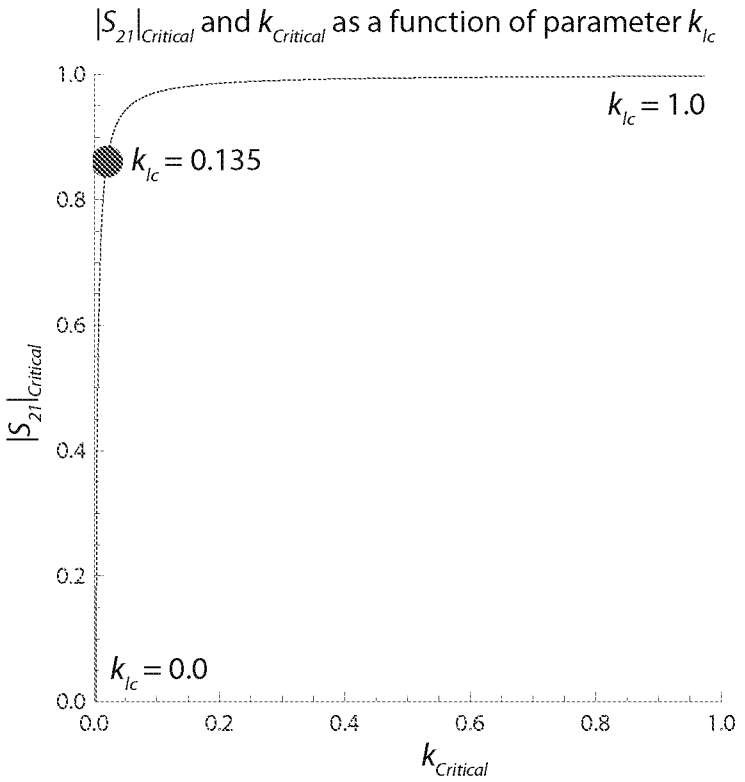
$|S_{21}|_{Critical}$ and $k_{Critical}$ as a function of parameter k_{lc}
$k_{lc} = 1.0$
$k_{lc} = 0.135$
$k_{lc} = 0.0$
$|S_{21}|_{Critical}$
$k_{Critical}$
0.0
0.2
0.4
0.6
0.8
1.0

FIGURE 6a

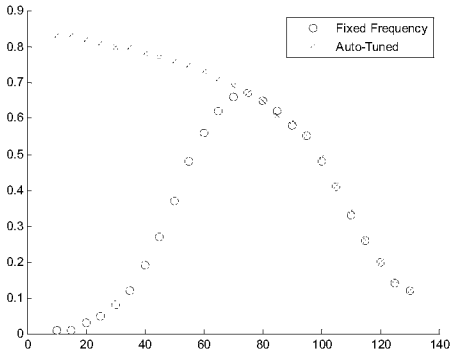

FIGURE 6b

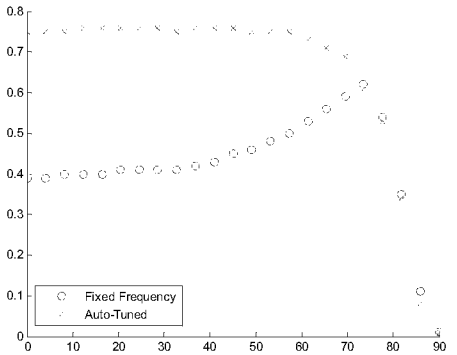

FIGURE 7

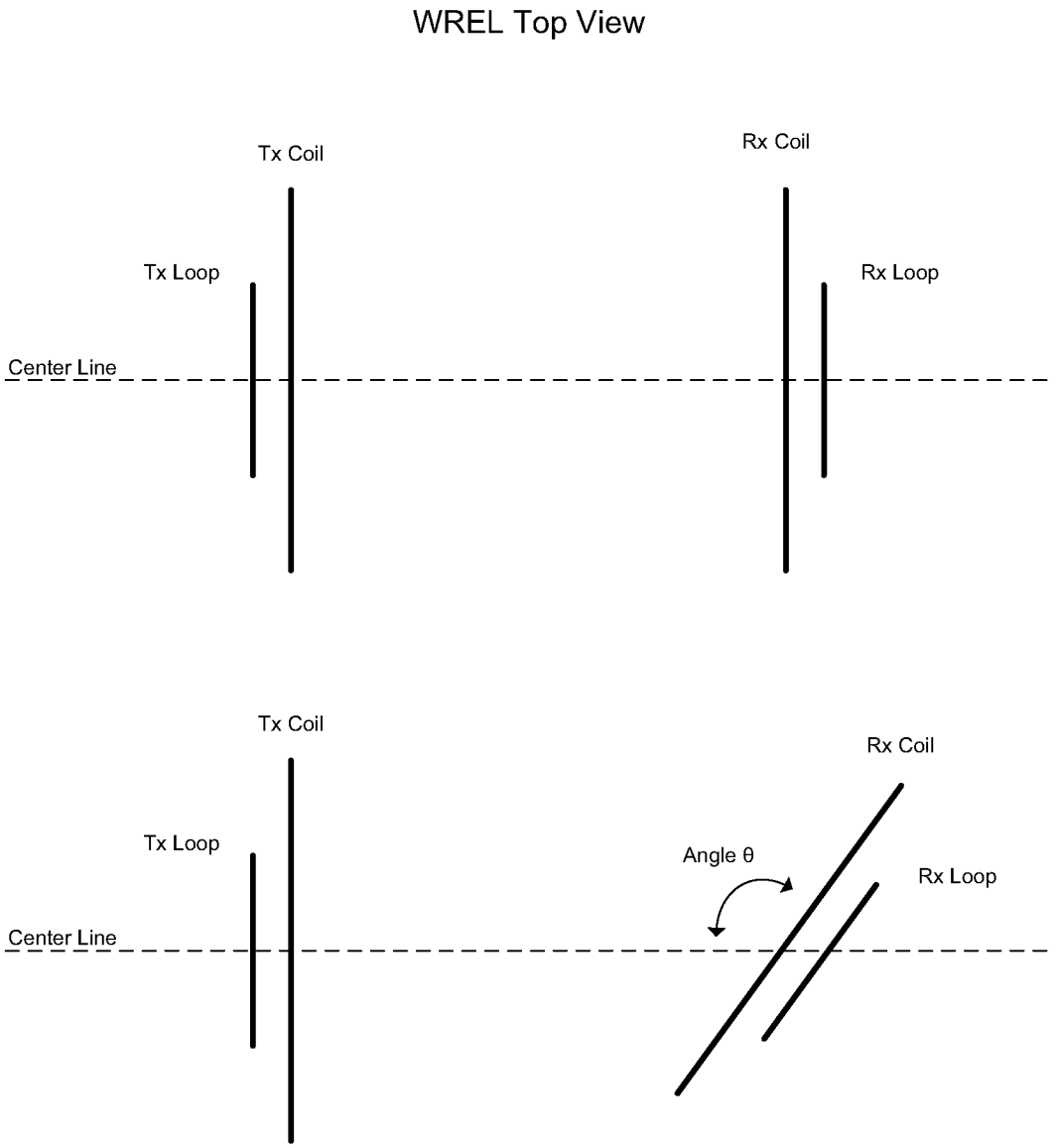
WREL Top View
Tx Coil
Rx Coil
Tx Loop
Rx Loop
Center Line
Tx Coil
Rx Coil
Tx Loop
Angle θ
Rx Loop
Center Line

FIGURE 8

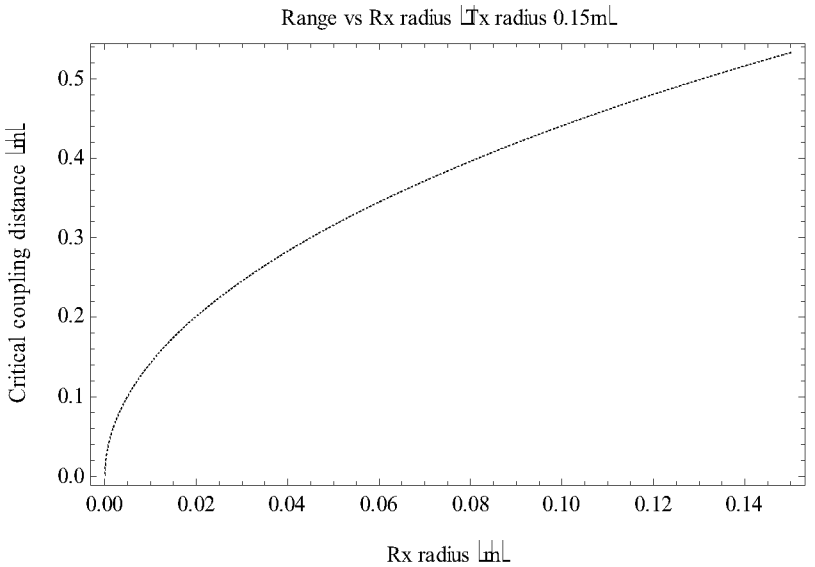

Range (Critical coupling distance) vs. Rx radius, for Tx radius = 0.15m.

FLAT, ASYMMETRIC, AND E-FIELD CONFINED WIRELESS POWER TRANSFER APPARATUS AND METHOD THEREOF

CROSS REFERENCE TO RELATED APPLICATIONS

This application claims benefit under 35 U.S.C. §119(e) from U.S. Provisional Application No. 61/189,502 filed on Aug. 20, 2008, incorporated herein by reference in its entirety.

BACKGROUND

This disclosure relates generally to the field of power transmission, and in particular, to a method and apparatus for transmitting and receiving power wirelessly.

Wireless power transfer has the potential to transform electronics by "cutting the last cord," freeing users from the need to plug in to recharge devices, and changing the design space, for example by enabling devices with no connectors.

Coupled resonator wireless power transfer is capable of delivering power with more efficiency than far field approaches and at longer range than traditional inductive schemes. However, conventional coupled resonator systems have been limited to operation at a particular fixed distance and orientation, with efficiency falling rapidly as the receiver moves away from the optimal operating point. Moreover, conventional coupled resonator systems use bulky, non-flat resonator structures.

BRIEF DESCRIPTION OF THE DRAWINGS

FIG. **1***a* shows an exemplary system diagram of an autotuning wireless power transfer system in accordance with various aspects of the present disclosure.

FIG. **1***b* shows an equivalent circuit diagram for the exemplary system of FIG. **1***a* in accordance with various aspects of the present disclosure.

FIG. **1***c* shows a photograph of an experimental set-up of a Tx Loop and Tx Coil (left), and Rx Coil and Rx Loop (right) in accordance with various aspects of the present disclosure.

FIG. **2***a* shows a plot of $|S_{21}|$ as a function of frequency and Tx-Rx coupling (k_{23}) in accordance with various aspects of the present disclosure.

FIG. **2***b* shows a plot of $|S_{21}|$ as a function of k_{23} and k_{12} in accordance with various aspects of the present disclosure.

FIG. **3***a* shows a locally fit model comparing experimental data (black dots) to the elementary transfer function (dotted line), and to the complete transfer function (line), for the best fit value of k_{23} in accordance with various aspects of the present disclosure.

FIG. **3***b* shows a locally fit model comparing experimental S21 magnitude data (black dots) and analytical model (surface) computed from the complete transfer function, both plotted versus frequency and Tx-Rx distance in accordance with various aspects of the present disclosure.

FIG. **4***a* shows a model (lines) compared to experimental data (black circles), with k_{23} values calculated from geometry (not fit to data) where $|S_{21}|$ is plotted vs distance in accordance with various aspects of the present disclosure.

FIG. **4***b* shows the model of FIG. **4***a* where resonant peak locations are plotted as a function of distance in accordance with various aspects of the present disclosure.

FIG. **4***c* shows the model of FIG. **4***a* where resonant peak magnitudes are plotted as a function of distance in accordance with various aspects of the present invention.

FIG. **5** shows efficiency—range tradeoff: $|S_{21}|_{Critical}$ vs. $k_{Critical}$ tradeoff curve as a function of the tuning parameter k_{lc}, with our system's operating point indicated (large dot at k_{lc}=0.135) in accordance with various aspects of the present invention.

FIG. **6***a* shows an experimental implementation where tuning frequency compensates for range changes in accordance with various aspects of the present invention.

FIG. **6***b* shows the experimental implementation of FIG. **6***a* where tuning frequency compensates for orientation changes in accordance with various aspects of the present invention.

FIG. **7** shows a representative top view of the experimental implementation of FIG. **6***a* illustrating the varying orientation of the receiver (Rx Coil and Rx Loop) in accordance with various aspects of the present invention.

FIG. **8** shows a plot of range (critical coupling distance) vs. Rx radius, for Tx radius=0.15 m.

DETAILED DESCRIPTION

In the description that follows, like components have been given the same reference numerals, regardless of whether they are shown in different embodiments. To illustrate an embodiment(s) of the present disclosure in a clear and concise manner, the drawings may not necessarily be to scale and certain features may be shown in somewhat schematic form. Features that are described and/or illustrated with respect to one embodiment may be used in the same way or in a similar way in one or more other embodiments and/or in combination with or instead of the features of the other embodiments.

In accordance with various embodiments of this disclosure, a transmitter is disclosed that includes a substantially two-dimensional resonator structure including a flat coil; and an impedance-matching structure operably connected to the resonator structure, the transmitter configured to transmit power wirelessly.

In accordance with various embodiments of this disclosure, a receiver is disclosed that includes a substantially two-dimensional resonator structure including a flat coil; and an impedance-matching structure operably connected to the resonator structure, the receiver configured to receive power wirelessly.

In accordance with various embodiments of this disclosure, a method is disclosed that includes providing a substantially two-dimensional resonator structure comprising a flat coil; an impedance-matching structure operably connected to the resonator structure, transmitting or receiving power wirelessly by the two-dimensional resonator structure.

These and other features and characteristics, as well as the methods of operation and functions of the related elements of structure and the combination of parts and economies of manufacture, will become more apparent upon consideration of the following description and the appended claims with reference to the accompanying drawings, all of which form a part of this specification, wherein like reference numerals designate corresponding parts in the various Figures. It is to be expressly understood, however, that the drawings are for the purpose of illustration and description only and are not intended as a definition of the limits of claims. As used in the specification and in the claims, the singular form of "a", "an", and "the" include plural referents unless the context clearly dictates otherwise.

Turning now to the various aspects of the disclosure, a model is disclosed of coupled resonators in terms of passive circuit elements. The conventional analysis, based on coupled mode theory, is difficult to apply to practical systems in terms of quantities such as inductance (L), capacitance (C), and

resistance (R) that are measurable in the laboratory at high frequencies (HF band) that is herein disclosed. The disclosed model shows that to maintain efficient power transfer, system parameters must be tuned to compensate for variations in Transmit-to-Receive ("Tx-Rx") range and orientation.

FIG. **1***a* shows an exemplary system diagram of an auto-tuning wireless power transfer system in accordance with various aspects of the present disclosure. FIG. **1***b* shows an equivalent circuit diagram including four coupled resonant circuits for the exemplary system of FIG. **1***a*. FIG. **1***c* shows a photograph of an experimental set-up of a wireless power transfer apparatus including a Tx Loop and Tx Coil (left), and Rx Coil and Rx Loop (right).

Turning to FIG. **1***a*, one aspect of the present disclosure is shown. A transmitter **100** is configured to supply power wirelessly to a receiver **200**. The transmitter **100** is shown having a transmitter resonator or resonator of the transmitter **105** as a coil (Tx Coil). Similarly, the receiver **200** is shown having a receiver resonator or resonator of the receiver **205** as a coil (Rx Coil). In some aspects, the transmitter resonator (Tx Coil) and/or the receiver resonator (Rx Coil) is a substantially two-dimensional structure. The transmitter resonator (Tx Coil) is coupled to a transmitter impedance-matching structure **110**. Similarly, the receiver resonator (Rx Coil) is coupled to a receiver impedance-matching structure **210**. As shown in FIG. **1***a*, the transmitter impedance-matching structure **110** is a loop (Tx Loop) and the receiver impedance-matching structure **210** is a loop (Rx Loop). Other impedance-matching structures may be used for the transmitter **100**, the receiver **200**, or both which include a transformer and/or and an impedance-matching network. The impedance-matching network may include inductors and capacitors configured to connect a signal source to the resonator structure.

Transmitter **100** includes a controller **115**, a directional coupler **120** and a signal generator and radio frequency (RF) amplifier **125** which are configured to supply control power to a drive loop (Tx Loop). Impedance-matching structure **110** of the transmitter **100** such as drive loop or Tx Loop is configured to be excited by a source (not shown in FIG. **1***a*) with finite output impedance R_{source}. Signal generator **125** output is amplified and fed to the Tx Loop. Power is transferred magnetically from Tx Loop to Tx Coil to Rx Coil to Rx Loop, and delivered by ohmic connection to the load **215**.

If the system becomes mis-tuned because of a change in Tx-Rx distance, a reflection may occur on the transmitter side. The directional coupler **120** separates the reflected power from the forward power, allowing these quantities to be measured separately. The controller **115** adjusts transmit frequency to minimize the ratio of reflected to forward power, thereby retuning the system for the new working distance.

Turning to FIG. **1***b*, a simple one-turn drive loop (TxLoop) can be modeled as an inductor L_1 with parasitic resistance R_{p1}. For element i, distributed inductance is labeled L_i, distributed capacitance is C_i, and parasitic resistance is R_{pi}. The coupling coefficient for the mutual inductance linking inductor i to inductor j is labeled k_{ij}. Capacitor may be added to make drive loop (Tx Loop) resonant at a frequency of interest, bringing the net capacitance for the loop to C_1. Drive loop (Tx Loop) is powered by source (V_{Source}). Transmit coil (Tx Coil) may be a multi-turn air core spiral inductor L_2, with parasitic resistance R_{p2}. Capacitance C_2 of transmit coil (Tx Coil) is defined by its geometry. Inductors L_1 and L_2 are connected with coupling coefficient k_{12}, where

$$k_{ij} = \frac{M_{ij}}{\sqrt{L_i L_j}}$$

is the coupling coefficient linking inductors i and j, and M_{ij} is the mutual inductance between i and j. Note that $0 \leqq k_{ij} \leqq 1$. Coupling coefficient k_{12} is determined by the geometry of drive loop (Tx Loop) and transmit coil (Tx Coil). Receiver apparatus is defined similarly to the transmitter apparatus: L_3 is the inductance of receiver coil (Rx Coil) and L_4 is the inductance of load loop (Rx Loop). Transmitter coil (Tx Coil) and receiver coil (Rx Coil) are linked by coupling coefficient k_{23}, which depends on both Tx-Rx range and relative orientation. Drive loop (Tx Loop) and load loop (Rx Loop) may be configured to impedance match source and load to high Q resonators (Tx Coil and Rx Coil).

As discussed above, source and load loops (Tx Loop and Rx Loop) may be replaced by other impedance matching components. The Tx loop (or equivalent component) and Tx coil may both be embedded in the same piece of equipment (and likewise for the Rx coil and Rx Loop or equivalent component). Thus, coupling constants k_{12} and k_{34} are variables that the can be, in principle, controlled, unlike coupling constant k_{23}, which is an uncontrolled environmental variable determined by usage conditions.

Uncontrolled environmental parameters may include parameters such as a range between the transmitter resonator (Tx Coil) and the receiver resonator (Rx Coil), a relative orientation between the transmitter resonator (Tx Coil) and the receiver resonator (Rx Coil), and a variable load on the receiver resonator (Rx Coil). By way of a non-limiting example, a variable load can be a device that experiences variations in a power state, such as a laptop computer powering on, down, or entering stand-by or hibernate mode. Other examples, may include a light bulb having various illumination states, such as dim or full brightness.

System parameters, such as the coupling constants k_{12} and k_{34}, are variables that the can be, in principle, controlled and that we can be adjust to compensate for the changes in environmental parameters. Other such system parameters may include a frequency at which power is transmitted, an impedance of the transmitter resonator and an impedance of the receiver resonator.

Writing Kirchhoffs voltage law (KVL) for each of the sub-circuits in the FIG. **1***b* allows the current in each to be determine:

$$I_1\left(R_{Source} + R_{p1} + j\omega L_1 + \frac{1}{j\omega C_1}\right) + j\omega I_2 k_{12}\sqrt{L_1 L_2} = V_S$$

$$I_2\left(R_{p2} + j\omega L_2 + \frac{1}{j\omega C_2}\right) + j\omega\left(I_1 k_{12}\sqrt{L_1 L_2} - I_3 k_{23}\sqrt{L_2 L_3}\right) = 0$$

$$I_3\left(R_{p3} + j\omega L_3 + \frac{1}{j\omega C_3}\right) + j\omega\left(I_4 k_{34}\sqrt{L_3 L_4} - I_2 k_{23}\sqrt{L_2 L_3}\right) = 0$$

$$I_4\left(R_{Load} + R_{P4} + j\omega L_4 + \frac{1}{j\omega C_4}\right) + j\omega I_3 k_{34}\sqrt{L_3 L_4} = 0$$

Solving these four KVL equations simultaneously for the voltage across the load resistor yields the transfer function for this system of coupled resonators:

$$V_{Gain} \equiv \frac{V_{Load}}{V_{Source}} = \frac{i\omega^3 k_{12}k_{23}k_{34}L_2L_3\sqrt{L_1L_4}\,R_{Load}}{k_{12}^2k_{34}^2L_1L_2L_3L_4\omega^4 + Z_1Z_2Z_3Z_4 + \omega^2(k_{12}^2L_1L_2Z_3Z_4 + k_{23}^2L_2L_3Z_1Z_4 + k_{34}^2L_3L_4Z_1Z_2)} \quad (1)$$

where V_{Load} is the voltage across the load resistor and

$$Z_1=(R_{p1}+R_{Source}+i\omega L_1-i/(\omega C_1))$$

$$Z_2=(R_{p2}+i\omega L_2-i/(\omega C_2))$$

$$Z_3=(R_{p3}+i\omega L_3-i/(\omega C_3))$$

$$Z_4=(R_{p4}+R_{Load}+i\omega L_4-i/(\omega C_4))$$

The analytical transfer function was cross-validated by comparing its predictions with SPICE (Simulation Program with Integrated Circuit Emphasis) simulations. As is known, SPICE is a general-purpose analog electronic circuit simulator that is used in integrated circuit (IC) and board-level design to check the integrity of circuit designs and to predict circuit behavior. From Eq. 1, a scattering parameter S_{21} can be calculated and shown to be:

$$S_{21} = 2\frac{V_{Load}}{V_{Source}}\left(\frac{R_{Source}}{R_{Load}}\right)^{1/2} \quad (2)$$

which can be important experimentally since it can be measured with a vector network analyzer, which as known, is an instrument used to analyze the properties of electrical networks, especially those properties associated with the reflection and transmission of electrical signals known as scattering parameters (S-parameters). The entire wireless power transfer apparatus can be viewed as a two-port network (one port being the input, fed by source, and the other the output, feeding the load). In a two-port network, S_{21} is a complex quantity representing the magnitude and phase of the ratio of the signal at the output port to the signal at the input port. Power gain, the essential measure of power transfer efficiency, is given by $|S_{21}|^2$, the squared magnitude of S_{21}. As presented below, experimental and theoretical results are presented in terms of $|S_{21}|$.

In FIG. **2***a*, $|S_{21}|$ is plotted for a realistic set of parameters, as shown in Table S1 below, as a function of the Tx-Rx coupling constant k_{23} and the driving angular frequency ω. In this plot, k_{12} and k_{34} are held constant, which would typically be the case for a fixed antenna design. This elementary transfer function neglects parasitic coupling, such as that from the drive loop (Tx Loop) direct to the receiver coil (Rx Coil), i.e. the k_{13} coupling. A more complete model that includes parasitic effects will be discussed later. However, the elementary model captures the essential behavior and is likely to be useful long term, as future systems may have reduced parasitic coupling.

FIG. **2***a* shows the dependence of system efficiency on frequency and k_{23}. On the k_{23} axis, smaller values correspond to larger Tx-Rx distances because the mutual inductance between the transmitter coil (Tx Coil) and receiver coil (Rx Coil) decreases with distance. Changing the angle of the receiver coil (Rx Coil) with respect to the transmitter coil (Tx Coil) can also change k_{23}. For example, rotating an on-axis receiver coil (Rx Coil) from being parallel to the transmitter coil (Tx Coil) to being perpendicular would decrease their mutual inductance and therefore k_{23}. Moving the receiver coil (Rx Coil) in a direction perpendicular to the transmit axis would also typically change k_{23}.

FIG. **2***a* shows the plot partitioned into 3 regimes, corresponding to different values of k_{23}. In the overcoupled regime, represented in FIG. **2***a* as the dotted lines that enclose the V-shaped ridge, $k_{23}>k_{Critical}$. (The value of the constant $k_{Critical}$ will be defined below in terms of the features of the surface plotted in the figure.) In the critically coupled regime, which is the plane bounding this volume, $k_{23}=k_{Critical}$. In the under-coupled regime beyond the volume outlined by the dotted lines, $k_{23}<k_{Critical}$.

High efficiency of power transmission occurs on the top of the V-shaped ridge. The V-shape is due to resonance splitting: in the over-coupled regime (i.e. for any choice of $k_{23}>k_{Critical}$) there are two frequencies at which maximum power transfer efficiency occurs. These correspond to the system's two normal modes. The more strongly coupled the resonators (transmitter coil (Tx Coil) and receiver coil (Rx Coil)) are, the greater the frequency splitting; the difference between the two normal mode frequencies increases with k_{23}. As k_{23} decreases, the modes move closer together in frequency until they merge. The value of k_{23} at which they merge (the point denoted by "I" on the V-shaped ridge) is defined to be the critical coupling point $k_{Critical}$. The frequency at which the modes merge is the single resonator natural frequency $\omega=\omega_0$ (assuming both coils have the same ω_0). Note that the mode amplitude is nearly constant throughout the over-coupled and critically coupled regime, allowing high efficiency; as k_{23} drops below $k_{Critical}$, the single mode amplitude decreases, lowering the maximum system efficiency achievable.

Because of the nearly constant mode amplitude throughout the overcoupled regime, system efficiency could be kept nearly constant as k_{23} varies (as long as $k_{23}>k_{Critical}$), if the system transmit frequency could be adjusted to keep the operating point on top of the ridge. In other words, as the Tx-Rx distance (and thus k_{23}) changes due to motion of the receiver, the system could be re-tuned for maximum efficiency by adjusting the frequency to keep the operating point on the top of the ridge.

As disclosed below, tuning transmitter resonator (Tx Coil) automatically to maximize transmission power can be achieved based on thee results. Because the tuning compensates for changes in k_{23}, the same technique can compensate for any geometrical variation that changes k_{23} (by a sufficiently small amount), including changes in orientation, and non-range changing translations.

A correctly functioning control system may allow the system efficiency to be nearly independent of range, for any range up to the critical range. It may be counter-intuitive that power transfer efficiency can be approximately independent of range (even within a bounded working region), since the power delivered by far-field propagation depends on range r as $1/r^2$, and traditional non-adaptive inductive schemes have $1/r^3$ falloff. Therefore, the top of the efficiency ridge, along which the efficiency is approximately constant is referred to as the "magic regime" for wireless power transfer. The values of k_{23} that the magic regime spans are given by $k_{Critical}\leqq k_{23}\leqq 1$. Thus, the smaller $k_{Critical}$, the larger the spatial extent spanned by the magic regime, and thus the larger the system's effective working range.

In FIG. **2***b*, frequency is held constant while k_{12} (and k_{34} constrained for simplicity to equal k_{12}) is varied. Adapting k_{12} to compensate for detuning caused by changes in k_{23} is another method for adapting to varying range and orientation.

Further analysis of the transfer function (Eq. 1) gives insight into the effect of circuit parameters on the performance of the wireless power system. As explained above, the effective operating range is determined by the value of $k_{Critical}$: the smaller $k_{Critical}$, the greater the spatial extent of the magic regime.

So, to understand system range, it will be useful to solve for $k_{Critical}$ in terms of design parameters. First, the transfer function can be clarified by substituting expressions for quality factor:

$$Q_i = \frac{1}{R_i}\sqrt{\frac{L_i}{C_i}} = \frac{\omega_0^i L_i}{R_i} = \frac{1}{\omega_0^i R_i C_i}, \text{ where } \omega_0^i = \frac{1}{\sqrt{L_i C_i}}$$

is the uncoupled resonant frequency of element i.

For simplicity, consider a symmetrical system, with the quality factor of the Tx and Rx coils equal, $Q_{Coil}=Q_2=Q_3$, and the quality factors of the Tx and Rx loops equal, $Q_{Loop}=Q_1=Q_4$. The symmetric loop-to-coil coupling $k_{12}=k_{34}$ will be denoted k_{lc}. Also it is assumed that $R_{Source}=R_{Load}$, $R_{p1}<R_{Source}$, $R_{p4}<R_{Load}$, and that the uncoupled resonant frequencies are equal: $\omega_0^i=\omega_0$ for all i. To find an expression for the critical coupling value, consider the transfer function when the system is driven at frequency $\omega=\omega_0$. This corresponds to a 2D slice of FIG. **2***a* along the center frequency of 10 MHz, whose apex is the critical coupling point of the system. Using the expressions for ω in terms of Q above, this slice of the transfer function can be written

$$V_{Gain|\omega=\omega_0} = \frac{ik_{23}k_{lc}^2 Q_{Coil}^2 Q_{Loop}^2}{k_{23}^2 Q_{Coil}^2 + (1 + k_{lc}^2 Q_{Coil} Q_{Loop})^2} \tag{3}$$

To derive an expression for $k_{Critical}$ the maximum of Eq. 3 is found by differentiating with respect to k_{23}. Then $k_{Critical}$ is the point along the k_{23} axis of FIG. **2***a* that (for positive values of k and Q) sets this derivative to zero:

$$k_{Critical} = \frac{1}{Q_{Coil}} + k_{lc}^2 Q_{Loop} \tag{4}$$

Finally, $k_{Critical}$ is substituted for k_{23} in Eq. 3 to find the voltage gain at the critical coupling point: $V_{GainCritical}=ik_{lc}^2Q_{Coil}Q_{Loop}/2(1+k_{lc}^2Q_{Coil}Q_{Loop})$. Using Eq. 2, and assuming that $R_{load}=R_{source}$, this voltage gain can be converted into $|S_{21}|$, which will be convenient to abbreviate $G_{Critical}$:

$$G_{Critical} \equiv |S_{21}|_{Critical} = \frac{k_{lc}^2 Q_{Coil} Q_{Loop}}{1 + k_{lc}^2 Q_{Coil} Q_{Loop}} = \frac{k_{lc}^2 Q_{Loop}}{k_{Critical}} \tag{5}$$

This equation quantifies the system's efficiency at the furthest point on the magic regime ridge. Recall that in order to maximize range, we must minimize $k_{Critical}$ because this increases the extent of the magic regime, which spans from $k_{Critical}$ to 1.0. Examining Eq. 4, reducing k_{lc} lowers $k_{Critical}$ and therefore increases range. However, according to Eq. 5, reducing k_{lc} also reduces efficiency. Indeed, the choice of k_{lc} trades off the efficiency level in the magic regime (height of magic regime ridge) vs. the extent of the magic regime (spatial extent of magic regime, i.e. maximum range). FIG. **5** is a plot of this tradeoff curve, $|S_{21}|_{Critical}$ vs $k_{Critical}$ as a function of the common parameter k_{lc}.

The area under this tradeoff curve serves as a useful figure of merit (FOM) for system performance:

$$FOM = \int_0^1 G_{Critical}\, dk_{Critical}.$$

An optimal wireless power system, which could losslessly deliver power at infinite range (0 coupling), would have an FOM of unity. For the symmetrical case (in which corresponding parameters on the transmit and receive sides are equal), the FOM integral can be evaluated analytically. Assuming that $Q_{Coil}>1$, the area under the tradeoff curve turns out to be

$$FOM = 1 - \frac{1}{Q_{Coil}} - \frac{\ln Q_{Coil}}{Q_{Coil}}. \tag{6}$$

The FOM turns out to depend only Q_{coil}, and is independent of Q_{Loop}. The quality factor of the resonators (coils) entirely determines this measure of system performance, which approaches to unity in the limit of infinite Q_{coil}. The measured Q_{Coil} values for the experimental system, which is discussed further below, are around 300 and 400, corresponding to FOM=0.978 and FOM=0.982 (plugging each Q_{coil} value into the symmetric FOM formula).

Choosing a feasible value of Q_{Loop} is the next important design question. To derive a guideline, an expression is found for the "knee" of the range-efficiency tradeoff curve, which we will define to be the point at which the slope

$$\frac{dG_{Critical}}{dk_{Critical}}$$

equals unity. The value of $k_{Critical}$ at which this occurs turns out to be

$$k_{CriticalKnee}=Q_{Coil}^{-1/2} \tag{7}$$

If Q_{Loop} is too small, then even setting k_{lc} to its maximum value of 1.0, $k_{Critical}$ will not be able to reach $k_{CriticalKnee}$. To find the minimum necessary Q_{Loop} value, Eq. 4 can be solved for Q_{Loop} with $k_{Critical}=k_{CriticalKnee}$ and $k_{lc}=1$, which yields $Q_{Loop}=(Q_{Coil}^{1/2}-1)Q_{Coil}^{-1}\approx Q_{Coil}^{-1/2}$ for large Q_{Coil}. Specifically, a good operating point on the tradeoff curve should be achievable as long as $Q_{Loop}>Q_{Coil}^{-1/2}$. For $Q_{Coil}=300$, this condition becomes $Q_{Loop}>0.06$.

A conclusion is that Q_{Coil} determines system performance (as measured by our FOM), as long as a minimum threshold value of Q_{Loop} is exceeded. The actual value of Q_{Loop} is dominated by the source and load impedances. The larger Q_{Coil} is, the smaller the required minimum Q_{Loop}. Conversely, moving to a more demanding load (with Q_{Loop} below the current threshold value) could be accomplished by sufficiently increasing Q_{Coil}.

Turning now to FIG. **1***c* which shows an experimental validation of the model. FIG. **1***c* shows transmitter coils (Tx Coil) and receiver coils (Rx Coil) that was used to validate the theoretical model, and to implement automatic range and orientation tuning. The transmitter on the left includes a small drive loop (Tx Loop) centered within a flat spiral transmit resonator (Tx Coil); the receiver side loop (Rx Loop) and coil (Rx Coil) are visible on the right. The system was characterized with a vector network analyzer in addition to the circuit values shown in Table S1 and S2, below. The first group of

measurements consisted of S_{11} measurements; the S_{11} scattering parameter is the ratio of complex reflected voltage to complex transmitted voltage at the input port. The ratio of reflected to transmitted power is given by $|S_{11}|^2$. L, C, and R values were extracted for each loop by fitting a model with these parameters to the S_{11} data. The second group of measurements was S_{11} measurements of the Tx Loop coupled to the Tx Coil, and corresponding measurements on the receiver side. Values were extracted for coil resonant frequency f_0 and Q, as well as loop-coil coupling coefficients k_{12} and k_{34}, again by fitting a model to data from both groups of measurements. It is not likely to extract L, C, and R values for the coils from these measurements because more than one parameter set is consistent with the data. So, an inductance value was calculated numerically for the coils based on their geometry, which then allowed C and R values to be calculated given the Q and f values.

The distance-dependent coupling coefficients are k_{23} (the main coil to coil coupling constant), and the parasitic coupling terms k_{13}, k_{24}, and k_{14}. To measure these, vector S_{21} data (not just $|S_{21}|$) was collected at a variety of Tx-Rx ranges for the complete 4 element system. Then at each distance, a non-linear fit was performed to extract the coupling coefficients. As an alternative method for finding the coupling coefficients, Neumann's formula was used to calculate the coupling coefficients directly from geometry.

Table S1 shows circuit values used to evaluate the elementary model.

TABLE S1

PARAMETER	Value
R_{source}, R_{Load}	50 Ω
L_1, L_4	1.0 uH
R_{p1}, R_{p4}	0.25 Ω
K_{12}, K_{34}	0.10
L_2, L_3	20.0 uH
C_2, C_3	12.6 pF
R_{p2}, R_{p3}	1.0 Ω
K_{23}	0.0001 to 0.30
f_0	10 MHz
Frequency	8 MHz to 12 MHz

It is to be noted that the expression for $k_{Critical}$ (Eq. 4) specifies the value of k_{23} that would be required to achieve critical coupling; it is not the case that the required coupling is achievable for all choices of Q, since only values corresponding to $k_{23} \leqq 1$ are realizable. Since all quantities in Eq. 4 are positive, it is clearly necessary (though not sufficient) that $1/Q_{Coil} \leqq 1$ and that $k_{lc}^2 Q_{Loop} \leqq 1$ for a realizable $k_{Critical}$ to exist. If a realizable $k_{Critical}$ does not exist, then there is no tuning that will allow the system to achieve the full efficiency of the magic regime; even when the system is maximally coupled, so that $k_{23}=1$, the system would operate in the sub-optimal under-coupled regime. It is to be noted that in practice it may not be possible to achieve $k_{lc}=1$, which would then require a larger minimum value of Q_{Loop}. Also, it is merely a coincidence that the minimum value of Q_{Loop} happens to be numerically so close to the value of $k_{CriticalKnee}$, since these are logically distinct.

To evaluate the integral of the parametric curve $G_{Critical}$ vs $k_{Critical}$ (both of which are parameterized by k_{lc}), k_{lcMax} is solved for in Eq. 4, the value of the parameter k_{lc} corresponding to the upper integration limit $k_{Critical}=1.0$, finding

$$k_{lcMax} = \sqrt{\frac{Q_{Coil}-1}{Q_{Loop}Q_{Coil}}}.$$

The correct lower integration limit is $k_{lc}=0$. So,

$$FOM = \int_0^{k_{lcMax}} G_{Critical} \frac{dk_{Critical}}{dk_{lc}} dk_{lc}, \text{ with } \frac{dk_{Critical}}{dk_{lc}} = 2k_{lc}Q_{Loop}.$$

Note that the power vs. range tradeoff does not indicate that power deliverable falls as the receiver moves further from the transmitter; it indicates that choice of k_{lc} trades off the extent of the "magic regime" (width of the magic regime plateau) with the amount of power delivered within the magic regime (height of the plateau).

The model was experimental validation using a drive loop that was 28 cm in diameter, with a series-connected variable capacitor used to tune the system to about 7.65 MHz. A SubMiniature version A (SMA) connector was also placed in series so that a RF amplifier was able to drive the system as described in FIG. **1***a*. The large transmitter coil started with an outer diameter of 59 cm and spiraled inwards with a pitch of 1 cm for approximately 6.1 turns. It was difficult to accurately predict the self capacitance of the coils, so the resonant frequency was tuned by manually trimming the end of the spiral until it resonates at ~7.65 MHz. The receiver was constructed similarly although minor geometrical differences which resulted in the Rx coils having roughly 6.125 turns after being tuned to ~7.65 MHz. All the elements were made of 2.54 mm diameter copper wire, supported by Plexiglas armatures.

A first group of measurements of the experimental set-up included S_{11} measurements (where S_{11} is the ratio of reflected voltage to transmitted voltage at the input port) of the Tx loop (denoted Measurement 1T in Table S2) and Rx loop (Measurement 1R), without the coils. From these, L, C, and R values were extracted for the loops by least squares fitting. The second group of measurements were S_{11} measurements of the Tx loop coupled to the Tx coil (Measurement 2T), and a corresponding receiver-side measurement denoted 2R. Using data from the second group of measurements and the previously extracted loop parameters, values were extracted for coil resonant frequency f_0 and Q, as well as loop-coil coupling coefficients k_{12} and k_{34}. It was not possible to extract L, C, and R values from these measurements. So, an inductance value for the coils based on their geometry was calculated numerically, which then allowed C and R values to be calculated.

Table S2 is shown below.

TABLE S2

MEASURED AND CALCULATED STATIC (NON-DISTANCE DEPENDENT) SYSTEM PARAMETERS

TRANSMITTER			RECEIVER		
COMPONENT	VALUE	SOURCE	COMPONENT	VALUE	SOURCE
L_1	0.965 uH	Measurement 1T	L_4	0.967 uH	Measurement 1R
C_1	449.8 pF	Measurement 1T	C_4	448.9 pF	Measurement 1R

TABLE S2-continued

MEASURED AND CALCULATED STATIC (NON-DISTANCE DEPENDENT) SYSTEM PARAMETERS

TRANSMITTER			RECEIVER		
COMPONENT	VALUE	SOURCE	COMPONENT	VALUE	SOURCE
R_{p1}	0.622 Ω	Measurement 1T	R_{p4}	0.163 Ω	Measurement 1R
R_{source}	50 Ω	Manufacturer Spec	R_{load}	50 Ω	Manufacturer Spec
Q_1	0.91	$L_1, C_1, R_{p1}, R_{source}$	Q_4	0.93	$L_4, C_4, R_{p4}, R_{load}$
F_1	7.64 MHz	L_1, C_1	F_4	7.64 MHz	L_4, C_4
K_{12}	0.1376	Measurement 2T; L_1, C_1, R_{p1}	K_{34}	0.1343	Measurement 2R; L_4, C_4, R_{p4}
Q_2	304.3	Measurement 2T; L_1, C_1, R_{p1}	Q_3	404.4	Measurement 2R; L_4, C_4, R_{p4}
F_{o2}	7.66 MHz	Measurement 2T; L_1, C_1, R_{p1}	F_{o3}	7.62 MHz	Measurement 2R; L_4, C_4, R_{p4}
L_2	39.1 uH	Calculation 1T	L_3	36.1 uH	Calculation 1R
C_2	11.04 pF	L_2, F_{o2}	C_3	12.10 pF	L_3, F_{o3}
R_{p2}	6.19 Ω	L_2, F_{o2}, Q_2	R_{p3}	4.27 Ω	L_3, F_{o3}, Q_3

The experimental set-up showed that the system was able to perform adaptive frequency tuning for range-independent maximum power transfer. The lower frequency mode had a higher amplitude in the experimental set-up (partly because of the sign of the parasitic signals), so when splitting occurs, the lower mode was automatically selected. From this, the benefit of the frequency tuning is apparent at short range, because the frequency that was chosen for the non-adaptive case (7.65 MHz) was appropriate for the long range situation. However, if a different frequency had been chosen for the fixed case, the benefit could have been apparent at the longer ranges rather than the shorter range.

Note that increasing range and increasing angle mismatch both decrease k_{23}, and the range and orientation mismatch together diminish k_{23} further; thus if the receiver had been further away, orientation adaptation would not have succeeded over such a wide range of angles. For extreme values of receiver angle, discussed further below, the coupling k_{23} drops sufficiently that the system is no longer in the over-coupled regime, so there is no splitting and no change in optimal system frequency with coupling constant; thus the fixed and auto-tuning performance coincide.

FIG. **3***a* compares experimentally measured $|S_{21}|$ data to the simple model of Eq. 1, and to a more complete model that includes parasitic couplings. The Figure shows a comparison of experimental data (dots) to the elementary transfer function (dotted line), and to the complete transfer function (line), for the best fit value of k_{23}. The simple model neglects parasitic coupling and does not reproduce the amplitude difference between the upper and lower modes. The complete model reproduces this amplitude difference, which is explained by the phase of the parasitic (e.g. k_{13}) coupling terms relative to the non-parasitic terms (e.g. k_{23}) for the two resonant modes. The agreement between the complete model and the experimental data is excellent. The difference in the magnitude of the $|S_{21}|$ peaks for the upper and lower modes (in FIG. **3***a* visible in the experimental data and in the complete model, and not present in the elementary model) can be explained by considering the phase of the two modes.

Based on the dynamics of coupled resonators, the lower frequency mode that the current in the transmitter coil is expected to be approximately in phase with the current in the receiver coil; in the higher frequency mode, the coil currents are expected to be approximately anti-phase (180 degrees out of phase).

In the lower mode, in which the Tx coil and Rx coil are in phase, the parasitic feed-through from the drive loop to the Rx coil (associated with coupling constant k_{13}) contributes constructively to the magnitude of the current in the receive coil. In the upper mode, the Rx coil phase is inverted but the parasitic feed through is not, so the feed through interferes destructively with the Rx coil current. Similar arguments apply to the other parasitic couplings. The fact that the mode magnitude differences are modeled well only when parasitic couplings are included (as shown in FIG. **3***a*) supports this conclusion.

As disclosed above, other impedance-matching components such as discrete matching network or shielded transformer may be used to connect the source/load to the coils, eliminating inductively coupled loops. This would eliminate the cross coupling term and simplify the model, and possibly also simplify system construction. On the other hand, the parasitic feedthrough benefits system performance in the lower mode, and this benefit will be lost by eliminating the loop.

FIG. **3***b* shows experimental data and the theoretical model, using coupling coefficients extracted separately for each distance. Experimental S21 magnitude data (dots) and analytical model (surface) computed from the complete transfer function, both plotted versus frequency and Tx-Rx distance. Note that each distance slice in the analytical surface is for an independently fit value k_{23}. As discussed above, the dotted box encloses the over-coupled region. For distances between experimental measurements (i.e. between the contours), k_{23} values were interpolated linearly from neighboring k_{23} values. Results using k_{23} computed directly from geometry are presented in the FIGS. **4***a*, **4***b* and **4***c* discussed below.

FIGS. **4***a*, **4***b* and **4***c* compare experimental data to the model, using only calculated coupling coefficients in the model. The model (lines) compared to experimental data (circles), with k_{23} values calculated from geometry (not fit to data). FIG. **4***a* shows $|S_{21}|$ vs distance. Predicted maximum coupling point is plotted as a solid dot. FIG. **4***b* shows reso-

nant peak locations as a function of distance. Frequency splitting is apparent below a critical distance. This plot can be thought of as the ridge lines of FIG. **3***b* viewed from above. FIG. **4***c* shows resonant peak magnitudes as a function of distance. This plot can be thought of as the ridge lines of FIG. **3***b* viewed from the side. In the simple model, these two branches would have the same magnitude; including parasitic couplings accounts for the magnitude difference between the modes.

In FIGS. **4***a*, **4***b* and **4***c*, only the static system parameters were measured; the dynamic (distance-dependent) parameters were calculated. The agreement is generally good, although at close range the numerical calculations become less accurate. This may be because capacitive coupling effects, which were not modeled, become more significant at close range.

Adaptive frequency tuning may be implemented for range-independent maximum power transfer. When the system is mis-tuned, for example when a non-optimal frequency is chosen, the impedance mis-match causes a reflection at the transmitter side; when the system is optimally tuned, the ratio of reflected to transmitted power is minimized. Thus if the transmitter is capable of measuring S_{11}, and adjusting its frequency, it can choose the optimal frequency for a particular range or receiver orientation by minimizing S_{11} (that is, minimizing reflected and maximizing transmitted signals). FIGS. **6***a* and **6***b* show experimental data for power transfer efficiency from a non-adaptive (fixed frequency) system compared with efficiency data from a working frequency auto-tuning system.

For each distance, the system swept the transmit frequency from 6 MHz to 8 MHz and then chose the frequency with minimal $|S_{11}|$ to maximize efficiency. At the optimal frequency for each distance, the power delivered into a power meter was measured. The range of tuned values was 6.67 MHz to 7.66 MHz. Analogous results are shown in FIG. **6***b* for receiver orientation adaptation. The system efficiency is nearly constant over about 70 degrees of receiver orientation. Only in the range from 70 to 90 degrees does the power transfer efficiency fall toward zero. In both cases shown in FIGS. **6***a* and **6***b*, the fixed frequency chosen was the single coil resonant frequency (i.e. the under-coupled system frequency), so as the system leaves the overcoupled regime, the auto-tuned frequency coincides with the fixed frequency, and so the efficiencies coincide as well.

FIG. **7** shows a representative top view of the experimental implementation of FIG. **6***a* illustrating the varying orientation of the receiver (Rx Coil and Rx Loop) in accordance with various aspects of the present invention. As seen in the top of FIG. **7**, Rx Coil and Rx Loop are aligned in orientation with Tx Loop and Tx Coil along a center line. The bottom of FIG. **7** shows Rx Coil and Rx Loop rotated through an angle θ with respect to the center line. When the Rx Coil and Rx Loop are arranged as in the top of the Figure, θ=0°. If Rx Coil and Rx Loop were arranged parallel to the center line, then θ=90°.

A tracking scheme that is able to keep the system in tune if the receiver is moved sufficiently slowly, and an adaptation technique for narrowband operation are disclosed. Rather than considering k_{lc} to be a static design parameter to be optimized (as above), k_{lc} may be consider as a dynamically variable impedance matching parameter that can enable range adaptation without frequency tuning. If the system is driven at ω_0 (the un-coupled resonant frequency) even though it is actually over-coupled ($k_{23}>k_{Critical}$), frequency splitting will result in the system being off resonance, and little to no power will be transferred. To bring the efficiency of the system back to a maximum, k_{lc} can be decreased, causing $k_{Critical}$ in Eq. 4 to decrease, until k_{23}=k at which point maximum power transfer can resume. The inventors has we have successfully implemented a form of this tuning method in laboratory demonstration systems that allows tuning for a variety of Tx-Rx distances (k_{23} values) with a hand adjustment of a loop that can be rotated about its coil, changing k_{lc}. The k_{lc} adaptation method has the advantage of allowing operation at a single frequency ω_0, which would be advantageous for band-limited operation. Thus, it is of practical interest to develop electronically controllable techniques for k_{lc} tuning. As noted earlier, the system's loops could be replaced by discrete matching networks; making these matching networks electronically variable could allow automatic k_{lc} tuning.

By way of a non-limiting example of the tracking and tuning scheme, a value of a loop-to-coil coupling coefficient of the transmitter resonator may be fixed and a frequency may be tune adaptively to choose a desired frequency for a particular value of a transmitter resonator coil-to-receiver resonator coil coupling coefficient. Reflected power may be monitored by the transmitter, for example, and a frequency of the transmitter resonator can be adjusted to minimize the reflected power. In some aspects, the transmitter resonator may sweep through a range of frequencies until the transmitter resonator receives a feedback signal from the receiver resonator. A desired frequency may be determined for a distance between the transmitter resonator and the receiver resonator based on the received feedback signal. The feedback signal may include signals such as a radio signal, WiFi, Bluetooth, Zigbee, RFID-like backscatter, or a load-modulated signal. The load-modulated signal may be modulated on a carrier signal of the transmitter resonator. In some aspects, a desired frequency may be determined for a distance between the transmitter resonator and the receiver resonator based on an impedance matching value between a signal source and a coil of the transmitter resonator.

As discussed above, the coupled resonator wireless power transfer system is capable of adapting to maintain optimum efficiency as range and orientation vary. This is practically important, because in many desirable application scenarios, the range and orientation of the receiver device with respect to the transmit device varies with user behavior. For example, a laptop computer being powered by a coil embedded in the wall of a cubicle would have a different range and orientation each time the user repositioned the device. One feature of the disclosed adaptation scheme is that the error signal for the control system can be measured from the transmitter side only. A separate communication channel to provide feedback from the receiver to the transmitter may not be required.

In some aspects, it is desirable to optimally power smaller size devices, such as hand held devices and scale the power transmitted based on the device size. Powering devices that are smaller than the transmitter is a case of practical interest: consider a computer display or laptop that recharges a mobile phone. The dependence of range on receiver coil size can be discussed by presenting the asymmetric form of Eq. 4, where the critical coupling (where asymmetric means that it is possible that $k_{12}\neq k_{34}$, $Q_1\neq Q_4$, and $Q_2\neq Q_3$):

$$k_{Critical} = \sqrt{\frac{(1+k_{12}^2 Q_1 Q_2)(1+k_{34}^2 Q_3 Q_4)}{Q_2 Q_3}} \leq 1 \tag{8}$$

For completeness an asymmetric form of Eq. 5 can be shown to be:

$$|S_{21}|_{Critical} = \frac{k_{12} k_{34} Q_1 Q_4 R_{Load}}{k_{Critical}\sqrt{L_1 L_4}\ \omega_0} \tag{9}$$

Insight into the scaling of range with coil sizes can be gained by starting from an approximate formula for coupling coefficient linking two single-turn coils. Although the coils as tested had five turns, the behavior is expected to be qualitatively similar. The formula assumes that the receive radius is less than the transmit radius ($r_{Rx}<r_{Tx}$) and that both are on-axis: $k(x)\approx(r_{Tx}^2 r_{Rx}^2)(r_{Tx}r_{Rx})^{-1/2}(x^2+r_{Tx}^2)^{-3/2}$. The distance of critical coupling (which measures range) can be solved as:

$$x_{Critical} = \left(\left(\frac{r_{Tx}}{k_{Critical}^{2/3}} - r_{Rx}\right) r_{Rx}\right)^{1/2} \tag{10}$$

into which the right hand side of Eq. 8 can be substituted. Substituting the measured values from Table S2 above into the right hand side of Eq. 8, substituting the resulting $k_{Critical}$ into Eq. 10, and assuming r_{Tx}=30 cm, plot of Eq. 10 is plotted in FIG. **8**. According to this plot, it may be possible to power a device of radius 5 cm from a transmitter of radius 15 cm at a range of about 30 cm. This parameter set may support the charging of a cell phone from a wireless power transmitter in a laptop computer.

In some aspects, Tx Coil and/or Rx Coil may be arranged as substantially flat or planar in design. In addition to improving integration with smaller and more planar-sized structure such as a laptop, a flat coil structure can also reduce unwanted spurious radio frequency (RF) emissions, because the substantially flat coil will have a smaller dipole moment in the direction perpendicular to the flat coil.

In some aspects, flat coils may be fabricated by forming a suitable number of turns of magnet wire, solid core wire, stranded wire, Litz wire, hollow copper tubing (producing better weight to conductivity ratio) on a non-conductive substrate or armature that maintains the appropriate flat geometry. Moreover, other methods of manufacturing a multi-turn 2D coil may be used including etched or otherwise patterned conductors and those manufactured by any methods used in printed circuit board fabrication.

In the embodiments herein, the apparatus could be manufactured by semiconductor device fabrication methods such as deposition, removal, patterning, and modification of electrical properties. Deposition methods, for example, include physical vapor deposition (PVD), chemical vapor deposition (CVD), electrochemical deposition (ECD), molecular beam epitaxy (MBE) and, atomic layer deposition (ALD) among others. Removal methods, for example, include wet etching, dry etching, chemical-mechanical planarization (CMP) among others. Patterning methods, for example, include lithography among others. Modification methods, for example, include reduction of dielectric constant via exposure to ultraviolet light in UV processing (UVP) among others.

Dielectric losses due to the armature materials may be minimized by eliminating all excess material not required for structural stability. The armature may be laser cut from acrylic or plastic, or injection molded plastic. The substrate may also be glass, plexiglass, Flame Retardant 4 (FR4), silicon, low-loss printed circuit board material, flexible printed circuit board material, polyamide, polycarbonate sold by, for example, Honlex Flexible PCB Industrial Co. Ltd of Taiwan.

Substantially flat coils for wireless power transfer may be fabricated by standard printed circuit board (PCB) fabrication methods: traces can be designed in standard CAD programs such as Altium Designer. Wider traces and thicker copper produce higher conductivity values, which provides for better resonator quality factor (Q), which in turn is a determinant of system range and efficiency. The resonator frequency is given by $f=1/(2\pi(LC)^{1/2})$; the resonator quality factor is given by $(1/R)(L/C)^{1/2}$. More turns provides additional inductance, which improves Q if C can be decreased to keep the desired resonant frequency f constant. At some point, the capacitance C can be decreased no further however, limiting the maximum inductance value that can be used for a particular resonant frequency f. An additional factor limiting the number of turns is that increased trace length increases resistance, which decreases Q. The need to increase L by using more turns limits the width of the traces. Balancing these factors has led the inventors to a design with around 6 turns, for operating frequencies in the range 5 MHz to 15 MHz.

Coils for wireless power transfer may also be fabricated using flexible printed circuit board (PCB) methods. Because the flexible PCB substrates are thinner than conventional circuit boards, they may be expected to cause less dielectric loss. PCB substrates made from low dielectric loss materials such as that from Rogers corporation may also be used to reduce dielectric losses. In a micro-electrical-mechanical systems (MEMS) process such as lithography, electroforming and molding (LIGA), thick (high aspect ratio) metal coils (which may be expected to have higher conductivity) may be fabricated on a silicon substrate.

The flat coils may also be fabricated by die stamping sheet metal; cutting metal foil using a vinyl cutter or similar tool; patterning metal using a waterjet, laser cutter, or saw. Flat coils may be fabricated from transparent conductors such as Indium Tin Oxide (ITO) or other Transparent Conductive Material.

Flat coils on the interior of a laptop lid may be patterned by screen printing, silk screening, stenciling, inkjet printing, or other processes capable of printing conductive materials.

The performance of the coils fabricated by several of the methods above can be improved by plating the materials with a higher conductivity, non-oxidizing materials such as silver, gold, or platinum. The coil performance can also be improved by increasing the amount or thickness of conductive material by electroplating or electroless plating (even if the plated material is not particularly high conductivity). The flat coils may be designed to receive power from outside the laptop, and shield emissions from inside. The outline of the 2-D coil is not limited to a specific shape and can adapt to mobile device design considerations, such as circular, rectangular, square or any other arbitrary shape in outline.

Although the above disclosure discusses what is currently considered to be a variety of useful embodiments, it is to be understood that such detail is solely for that purpose, and that the appended claims are not limited to the disclosed embodiments, but, on the contrary, is intended to cover modifications and equivalent arrangements that are within the spirit and scope of the appended claims.

What is claimed is:

1. A transmitter comprising:

a substantially two-dimensional resonator structure including a flat coil; and

an impedance-matching structure operably connected to the resonator structure, the transmitter configured to transmit power wirelessly,

wherein the substantially two-dimensional resonator structure provides a smaller dipole moment in a direction perpendicular to the resonator structure as compared to a non-two-dimensional resonator structure.

2. The transmitter according to claim **1**, wherein the impedance-matching structure includes one or more of the following: a loop, a transformer, and an impedance-matching network.

3. The transmitter according to claim 2, wherein the impedance-matching network includes inductors and capacitors configured to connect a signal source to the resonator structure.

4. The transmitter according to claim 1, wherein the transmitter is configured to draw energy to be transmitted from a power supply.

5. The transmitter according to claim 1, wherein the resonator structure includes a number of turns of a magnet wire, a solid core wire, a stranded wire, a Litz wire, a hollow copper tubing on a non-conductive substrate, an etched conductor or a patterned conductor.

6. The transmitter according to claim 5, wherein the non-conductive substrate includes acrylic, plastic, injection molded plastic, glass, plexiglass, Flame Retardant 4, silicon, low-loss printed circuit board material, flexible printed circuit board material, polyamide, polycarbonate, or a printed-circuit board.

7. The transmitter according to claim 1, wherein the resonator structure is arranged on an interior of a laptop lid.

8. The transmitter according to claim 1, wherein the resonator structure is arranged inside a mobile computing device.

9. The transmitter according to claim 1, wherein the resonator structure is patterned by screen printing, silk screening, stenciling or inkjet printing.

10. A receiver comprising:

a substantially two-dimensional resonator structure including a flat coil; and

an impedance-matching structure operably connected to the resonator structure, the receiver configured to receive power wirelessly,

wherein the substantially two-dimensional resonator structure provides a smaller dipole moment in a direction perpendicular to the resonator structure as compared to a non-two-dimensional resonator structure.

11. The receiver according to claim 10, wherein the impedance-matching structure includes one or more of the following: a loop, a transformer, and an impedance-matching network.

12. The receiver according to claim 11, wherein the impedance-matching network includes inductors and capacitors configured to connect a signal source to the resonator structure.

13. The receiver according to claim 10, wherein the receiver is arranged to be connected to an external load and is configured to power the load using the received power.

14. The receiver according to claim 10, wherein the resonator structure includes a number of turns of magnet wire, solid core wire, stranded wire, Litz wire, hollow copper tubing on a non-conductive substrate, or an etched conductor.

15. The receiver according to claim 14, wherein the non-conductive substrate includes acrylic, plastic, injection molded plastic, glass, plexiglass, Flame Retardant 4, silicon low-loss printed circuit board material, flexible printed circuit board material, polyamide, polycarbonate, or a printed-circuit board.

16. The receiver according to claim 10, wherein the resonator structure is arranged on an interior of a laptop lid.

17. The receiver according to claim 10, wherein the resonator structure is arranged inside a mobile device.

18. The receiver according to claim 10, wherein the resonator structure is patterned by screen printing, silk screening, stenciling or inkjet printing.

19. A method comprising:

providing a substantially two-dimensional resonator structure comprising a flat coil, and an impedance-matching structure operably connected to the resonator structure; and

transmitting or receiving power wirelessly by the two-dimensional resonator structure,

wherein the substantially two-dimensional resonator structure provides a smaller dipole moment in a direction perpendicular to the resonator structure as compared to a non-two-dimensional resonator structure.

20. The method according to claim 19, wherein the impedance-matching structure includes one or more of the following: a loop, a transformer, and a impedance-matching network.

21. The method according to claim 19, wherein the resonator structure includes a number of turns of a magnet wire, a solid core wire, a stranded wire, a Litz wire, a hollow copper tubing on a non-conductive substrate, an etched conductor or a patterned conductor.

22. The method according to claim 21, wherein the non-conductive substrate includes acrylic, plastic, injection molded plastic, glass, plexiglass, Flame Retardant 4, silicon, low-loss printed circuit board material, flexible printed circuit board material, polyamide, polycarbonate, or a printed-circuit board.

23. The method according to claim 19, further comprising patterning the resonator structure using screen printing, silk screening, stenciling or inkjet printing.

* * * * *